

Nonlinear Wave Forces on an Offshore Wind Turbine Foundation in Shallow Waters

Sung-Jin Choi¹, Kwang-Ho Lee^{2*}, Keyyoung Hong², Seong-Ho Shin²,
O.T. Gudmestad¹

¹*Department of Mechanical and Structure Engineering and Material Science, University of Stavanger, Norway*

²*Maritime & Ocean Engineering Research Institute, KIOST, Daejeon 305-343, Korea*

(Manuscript Received March 14 2013; Revised April 2, 2013; Accepted May 10, 2013)

Abstract

In this study, a 3D numerical model was used to predict nonlinear wave forces on a cylindrical pile installed in a shallow water region. The model was based on solving the viscous and incompressible Navier-Stokes equations for a two-phase flow (water and air) model and the volume of fluid method for treating the free surface of water. A new application was developed based on the cut-cell method to allow easy installation of complicated obstacles (e.g., bottom geometry and cylindrical pile) in a computational domain. Free-surface elevation, water particle velocities, and inline wave forces were calculated, and the results show good agreement with experimental data obtained by the Danish Hydraulic Institute. The simulation results revealed that the proposed model can, without the use of empirical formulas (i.e., Morison equation) and additional wave analysis models, reliably predict nonlinear wave forces on an offshore wind turbine foundation installed in a shallow water region.

Keywords: 3D numerical model, Nonlinear wave force, Cylindrical pile, Volume of fluid method, Cut-cell method

1. Introduction

Over the past few years, a large number of offshore wind turbines, which are mainly supported by typical mono-piles, gravity foundations, tripod structures, or jacket structures, have been developed or planned in order to harness abundant wind power. Most of these offshore wind turbines are likely to be installed in relatively shallow water regions because the cost of building and maintaining them and transmitting the power back to land increases with the distance from the shore. When an offshore wind turbine is installed in a shallow water region, the waves propagating toward the structure may experience severely nonlinear wave deformations, generating nonlinear waves that give rise to serious

concerns about the foundation. Therefore, in designing offshore wind turbines installed in shallow water regions, it is of great importance to accurately estimate the external wave force acting on them.

Until now, conventional methods such as combining a wave analysis model with a structural analysis model have mainly been used for estimating nonlinear wave forces acting on offshore structures installed in a shallow water region [7][8][19]. However, such methods appear to have problems with respect to accurate estimation of the nonlinear wave forces. First, most of the wave analysis models are based on shallow water equations—the simplest form of the equation of motion—derived from depth-integrating the Navier-Stokes equations. Although the wave models that use shallow water equations can simulate undisturbed wave kinematics occurring in the vicinity of the structural position to a reasonable degree, they are unlikely to be

*Corresponding author. Tel.: +82-42-866-3917, Fax.: +82-42-3919,

E-mail address: khlee@kiost.ac

Copyright © KSOE 2013.

sufficient for simulating strongly nonlinear interactions between waves and the structure in a shallow water region. Second, most of the structural analysis models use the Morison equation. However, in the Morison equation, the inertia and drag coefficients required to compute wave force seem to involve considerable uncertainties in their applications because they have been estimated from different experimental studies and field investigations. Furthermore, the estimated coefficients showed remarkable differences depending on the wave theories used in the experiments. With this in mind, the shore protection manual points out that, for force calculations, it is important to use a wave theory that is equivalent to the wave theory used to obtain the inertia and drag coefficients [5]. In addition to this constraint, the hydrodynamic coefficients depend greatly on the shape of the structure. For instance, if the shape of each member of the offshore wind turbine foundation is unique, the inertia and drag coefficients have to be estimated for each member on the basis of additional experimental approaches instead of using general values presented in methods such as API RP 2A-WSD [3], ISO 19902 [14], and DnV-RP-C205 [9].

The use of a computational fluid dynamics (CFD) computer model is an alternative method for overcoming such problems. In particular, numerical models that are based on the Navier-Stokes solver capable of solving nonlinear wave-structure interactions with high resolution are rapidly increasing with the expansion of computer resources [13][21]. Because the Navier-Stokes solver not only can specifically simulate strongly nonlinear characteristics of the waves occurring in the vicinity of the complex structure but also can calculate the wave forces by directly integrating the pressures along the structure surface, there is no need to use an empirical formula such as the Morison equation or additional wave analysis models.

The main objective of this study was to propose a 3D numerical model based on a numerical wave tank concept, which is a powerful tool that can efficiently and economically simulate flow fields under the same conditions as those in hydraulic experiments or field tests. Therefore, the developed numerical model can predict the nonlinear wave forces on an offshore wind turbine foundation installed in a shallow water region without the use of an em-

pirical formula and additional wave analysis models. In order to meet the goals of the present study, a 3D Navier-Stokes solver was used that was based on viscous and incompressible momentum equations for a two-phase flow (water and air) model and the volume of fluid (VOF) method. In particular, the complicated obstacles (e.g., the bottom geometry and the cylindrical pile) in the computational domain were embodied by the cut-cell method. The nonlinear wave forces on the cylindrical pile were calculated by using the proposed numerical model, and the calculated results were compared with experimental data obtained by the Danish Hydraulic Institute (DHI). Furthermore, the applicability of the developed numerical model for predicting the nonlinear wave forces is discussed.

2. Numerical Methodology

2.1 Governing equations

To investigate interactions between a cylindrical structure and waves, we adopted the numerical wave tank (NWT) method developed by Lee et al [17], which comprises an internal wave source for generating waves, an artificial damping zone (sponge layer) to prevent wave reflection at the lateral boundary, and a surface-tracking function for treating the evolution of the free surface of the water.

Assuming that the two fluids are viscous, incompressible, and immiscible, the fluid flow is governed by the continuity and the modified Navier-Stokes equations.

$$\frac{\partial(mv_j)}{\partial x_j} = q^* \quad (1)$$

$$\begin{aligned} m \frac{\partial v_j}{\partial t} + mv_i \frac{\partial v_j}{\partial x_i} \\ = -\frac{m}{\tilde{\rho}} \frac{\partial p}{\partial x_i} + \frac{\partial}{\partial x_j} (2\tilde{\nu}D_{ij} - \tau_{ij}) - Q_i - \beta_{ij}v_j + f_i \end{aligned} \quad (2)$$

where t is the time; $v_i = [u, v, w]^T$ is the velocity vector; p is pressure; $x_i = [x, y, z]^T$ is the position vector; m is the ratios of the fractional area open to the flow; f_i is the arbitrary body forces due to the effects of the gravity and surface tension; $D_{ij} = (\partial v_i / \partial x_j + \partial v_j / \partial x_i) / 2$ is the strain rate tensor; τ_{ij} is the turbulent stress based

on the Smagorinsky SGS model [20]; $\beta_{ij} = \beta \delta_{ij} \delta_{j3}$ is the dissipation factor matrix, in which β is the dissipation factor that equals 0 except in the added dissipation zone; $q^* = q(y, z; t) / \Delta x_s$ is the wave generation source; $\tilde{\rho}$ and $\tilde{\nu}$ are the density and kinematic viscosity averaged over the computational grid, respectively, which is determined as a linear sum of the local mass, using the volume-of-fluid (VOF) function of water, C .

$$\tilde{\rho} = C\rho_w + (1 - C)\rho_g \tag{3}$$

$$\tilde{\nu} = C\nu_w + (1 - C)\nu_g \tag{4}$$

where the subscriptions indicate each fluid phase. The value of the VOF function ranges between zero and unity, where unity occurs if the cell is completely filled with water, zero occurs if the cell is completely filled with air or an obstacle, and $0 < C < 1$ generates if the cell is filled partly with water and air. The wave source vector Q_i is formulated as follows:

$$Q_i = -\frac{2}{3} \frac{\partial(\tilde{\nu}q^*)}{\partial x_i} \tag{5}$$

where q^* is gradually increased for the initial three wave periods using an exponential function [4].

2.2 Free-surface elevation

In order to track the interface between two-phase flows, we used the original VOF method developed by Hirt and Nichols [11]. Although this method uses the simplified line interface calculation in interface reconstruction, its applicability has been demonstrated by many researchers [6][15][16]. In the VOF method, the interface between the water

and the air phase is modeled according to the VOF function, i.e., the VOF method evolves the volume of water in each cell over time instead of directly tracking the free surface itself. The advection of the VOF function is obtained by solving the conservation of fluid mass in each cell as follows:

$$\frac{\partial(mC)}{\partial t} + \frac{\partial(mv_j C)}{\partial x_j} = Cq^* \tag{6}$$

2.3 A new application based on the cut-cell method

To numerically solve the governing equations above, finite difference approximations were used in the fixed rectangular grid system. However, because the finite difference method depends on the grid quality in handling the obstruction installed in the calculation zone, its application will be restricted to simple geometry and the discontinuity of the obstacle surface by the rectangular cells can be generated in the vicinity of the obstacle. In order to overcome the drawback of using regular grid systems in incorporating complicated obstacles, a new application was developed based on the cut-cell method, which is essentially similar to the fraction area/volume obstacle representation (FAVOR) method, developed by Hirt and Sicilian [12], as shown in Figs. 1 and 2. This application records the following four parameters in each cell: the ratio of fractional volume open to flow, m_v ; the ratio of fractional area open to flow in each direction, m_x , m_y , and m_z ; the area of the wetted surface of the structure; and the unit normal vectors to the obstacle surfaces. The governing equations are formulated in terms of the computed four parameters to block portions of each cell containing the obstacle. Moreover, the calculated area of the wetted surface of the structure and the unit normal vectors were used to obtain the wave forces on the structure.

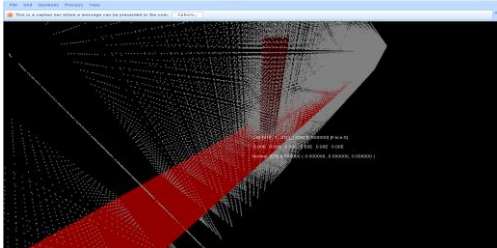


Fig. 1 Application of cut-cell method

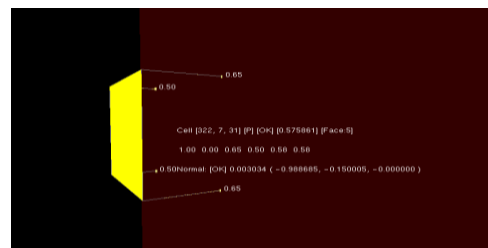


Fig. 2 Calculation results for grid information

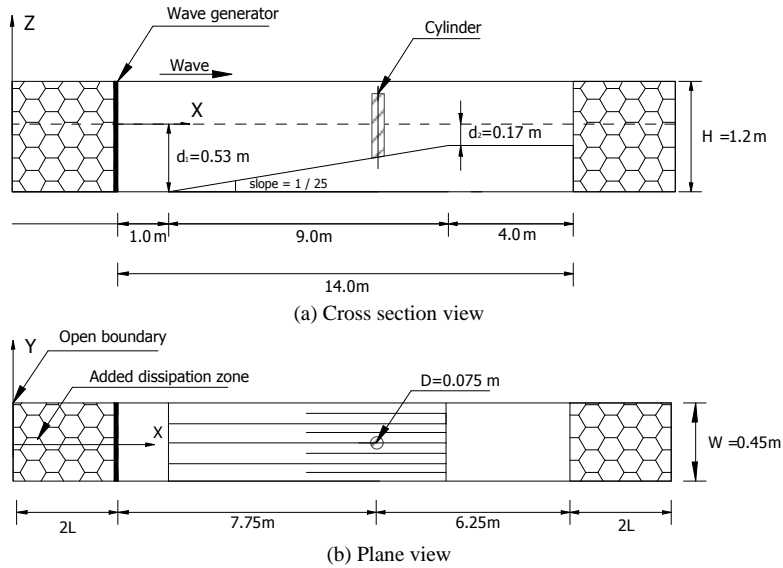


Fig. 3. Numerical Wave Tank

2.4 Boundary conditions

To treat the boundary of the calculation area, appropriate boundary conditions were adopted on the solid boundary and the lateral boundaries. There was no need to apply the free-surface boundary condition because the water and the air phase were modeled as a fluid in the two-phase flow model. For this reason, the dynamic boundary condition is automatically satisfied, whereas the kinematic boundary condition is satisfied by tracking the VOF function. As for the open boundary conditions, fictitious dissipation zones were added at both ends of the computational domain to control the reflected waves. To obtain an artificial damping effect, grids in the added fictitious dissipation zones were gradually coarsened toward the outmost open boundaries. Moreover, a non-gradient boundary condition was employed at the outer edges of the added fictitious dissipation zones. The pressure-constant con-

dition was applied to the top boundary condition. An impermeable condition (for normal velocities) and a slip condition (for tangential velocities) were imposed to treat the bottom boundary condition and the obstacle boundary condition, respectively.

2.5 Solution method

Finite difference approximations were used to calculate the governing equations and the VOF advection equation. A staggered mesh was used for the computational discretization to avoid the chess-board type solutions that can easily occur in the periodic pressure or velocity fields such as wave motion. For the staggered mesh pressure, the wave source function and the VOF function were computed at the cell center, whereas the velocity components were computed at the center of the cell face. The continuity equation was discretized by using the central difference method.

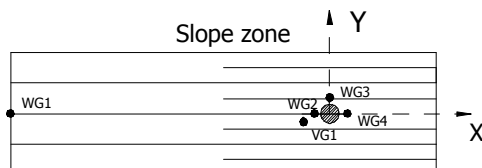


Fig. 4. Locations of the wave gauges and the velocity meter over the slope zone

Table 1. Measuring positions

	X(m)	Y(m)	Z(m)
WG1	-6.75	0.00	-
WG2	-0.15	0.00	-
WG3	0.00	0.15	-
WG4	0.20	0.00	-
VG1	-0.25	-0.05	0.46

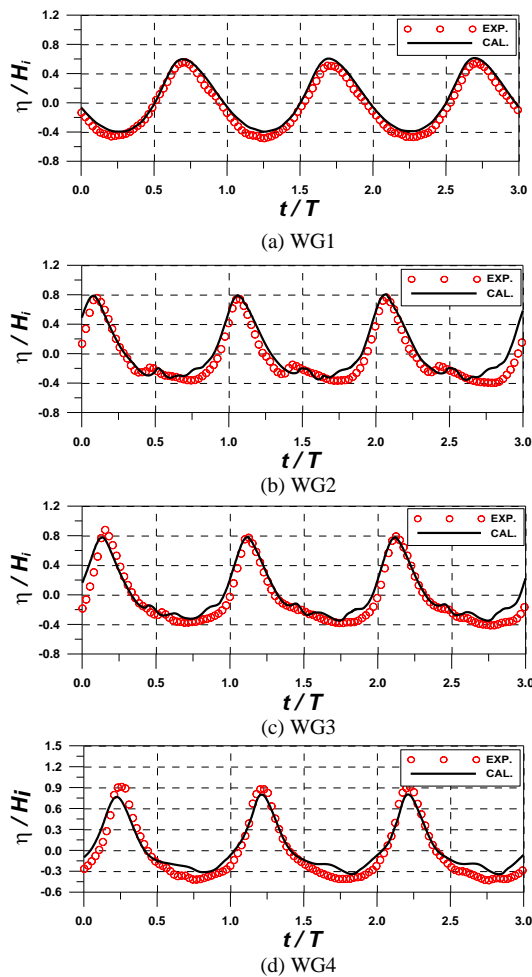


Fig. 5. Comparison of free-surface elevations between experimental measurements and the numerical results

For the discretization of the Navier-Stokes equations, the forward difference method for time derivative terms, constrained interpolation profile (CIP) method for the advection terms, the central difference method for the non-advection terms were employed. The velocity components and the pressure at the new time step can be estimated using the discretized momentum equations and suitable boundary conditions. However, the new time velocity components, which are estimated using the discretized momentum equations, do not generally satisfy the continuity equation in a controlled vol-

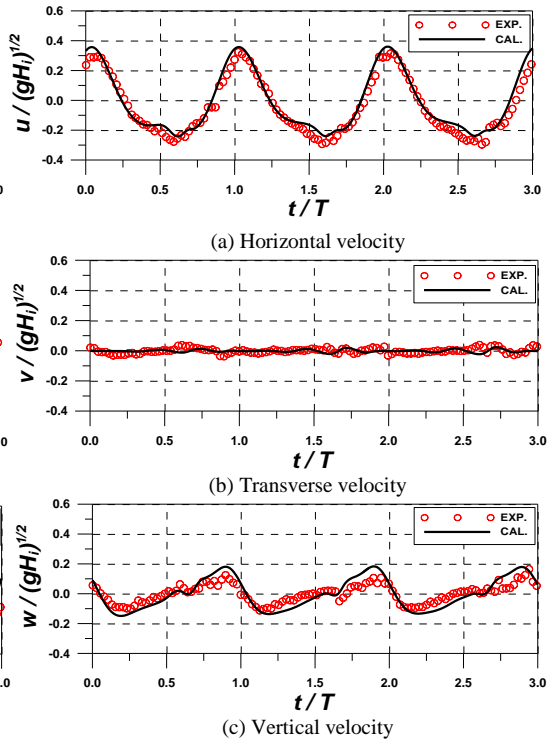


Fig. 6. Comparison of the time variations for water particle velocities

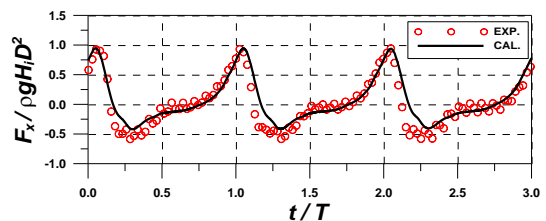


Fig. 7. Comparison of the time variations for inline wave forces

ume. Therefore, the simplified marker and cell (SMAC) method [2] was incorporated in order to iteratively adjust the velocities and the pressure in each cell until the continuity equation was reasonably satisfied. By using the SMAC method, the pressure correction can be obtained by solving a Poisson Pressure Equation (PPE). Then, the correct velocities at the new time step can be updated using the pressure correction computed by the PPE. In the present study, the PPE was solved by using the algebraic multi-grid (AP-AMG) solver, which was developed by Iwamura [1]. After the correct veloci-

ty components and pressure were determined, the new free-surface configuration was tracked by solving the advection equation for the VOF function using the updated velocity components.

3. Application of Numerical Analysis

3.1 Numerical Wave Tank Set-Up

An NWT similar to an experimental configuration was developed. Figure 3 shows the schematic of the NWT developed for this analysis. The length, width, and height of the NWT were 18.0 m, 0.45 m, and 1.2 m, respectively. In the NWT, the grid size varied from a minimum of $0.01 \times 0.01 \times 0.01$ m in the vicinity of the cylindrical pile to a maximum of $0.04 \times 0.01 \times 0.08$ m far from the cylindrical pile. The water depths were 0.53 m in front of the internal wave generator (d_1) and 0.17 m on the plateau (d_2). The slope of the bottom was considered to be 1/25. Added fictitious dissipation zones were located to the left and right sides of the computational domain with a thickness of $2L$, with L being the wave length, in order to absorb the wave energy. The internal wave generator (which can generate a regular wave train using a Stokes first order wave theory) was located in front of the added fictitious dissipation zone that was located at the left part of the computational domain. An incident wave condition (wave height $H_i = 0.138$ m and wave period $T = 1.565$ s) was considered in the numerical analysis among a total of 29 experimental conditions (regular wave conditions). A cylindrical pile with a diameter of 0.075 m was located 7.75 m from the internal wave generator. Three numerical wave gauges were used to measure the water surface elevations at the starting point of the sloping bottom (at WG 1) and near the cylindrical pile (at WG 2, WG 3, and WG 4). Moreover, the water particle velocities in the vicinity of the cylindrical pile (in the x-, y-, and z-directions) were measured using a numerical velocity meter (VG1). The correct locations of the velocity meter and the wave gauges (shown in Figure 4) are listed in Table 1.

3.2 Computational Results and Discussion

Fig. 5 shows the comparisons of the calculated and the measured free-surface elevations at WG 1, WG 2, WG 3, and WG 4. Four wave gauges are located at the starting point of the sloping bottom (at WG 1), in

front of the pile (at WG 2), at the left side of the pile (WG 3), and at the rear of the pile (WG 4) as already shown in Fig. 4. The free-surface displacements, which were measured in an experiment carried out at DHI (and computed) at all gauges, were normalized by the incident wave height. The red open circles represent the measured free-surface elevations and the black lines indicate the computed free-surface elevations. As the waves move over the sloping bottom, the wave profiles are transformed into typical shallow water waves (nonlinear effects becoming stronger) such that the wave crests are steeper and narrower with increased wave heights and the wave troughs are longer and flatter. These characteristics are evident in Figs 5(b)-(d). Overall, a reasonable agreement between the measured and the calculated free-surface elevations was observed. However, in point WG 4, the calculated results at both the wave crest and trough are slightly underestimated compared with the measured results. Meanwhile, it should be noted that, in WG 2, the slight ripples in the wave trough are reproduced relatively well in the numerical results, although a slight phase discrepancy is observed.

Fig. 6 represents the comparisons of the calculated water particle velocities (VG1 in the x-, y-, and z-directions) with the water particle velocities measured by using a Vectrino (Acoustic Doppler Velocity meter). The x-, y-, and z-coordinates of the Vectrino are respectively -0.25 m, -0.05 m, and 0.2 m away from the center of the pile. The ordinate in the figures is the velocity normalized by $(gH_i)^{1/2}$. In these figures, the black lines indicate the results found by the Navier-Stokes solver and the red open circles indicate the results measured by DHI. As waves move toward the cylindrical pile over the sloping bottom, the time variation of the water particle velocities becomes complex. Even so, several characteristic ripples were estimated fairly well in the time variation of the computed velocities. For the horizontal water particle velocity, the computations and measurements were in reasonable agreement, although there was a small gap between the calculated and the measured results at the velocity troughs. However, for the vertical water particle velocities, the calculated results at both the velocity crest and the trough were slightly overestimated compared with the experimental data. This slight discrepancy can be explained by the relatively coarse setup of the grid spacing, and it is thought that this discrepancy can be improved by using finer grids.

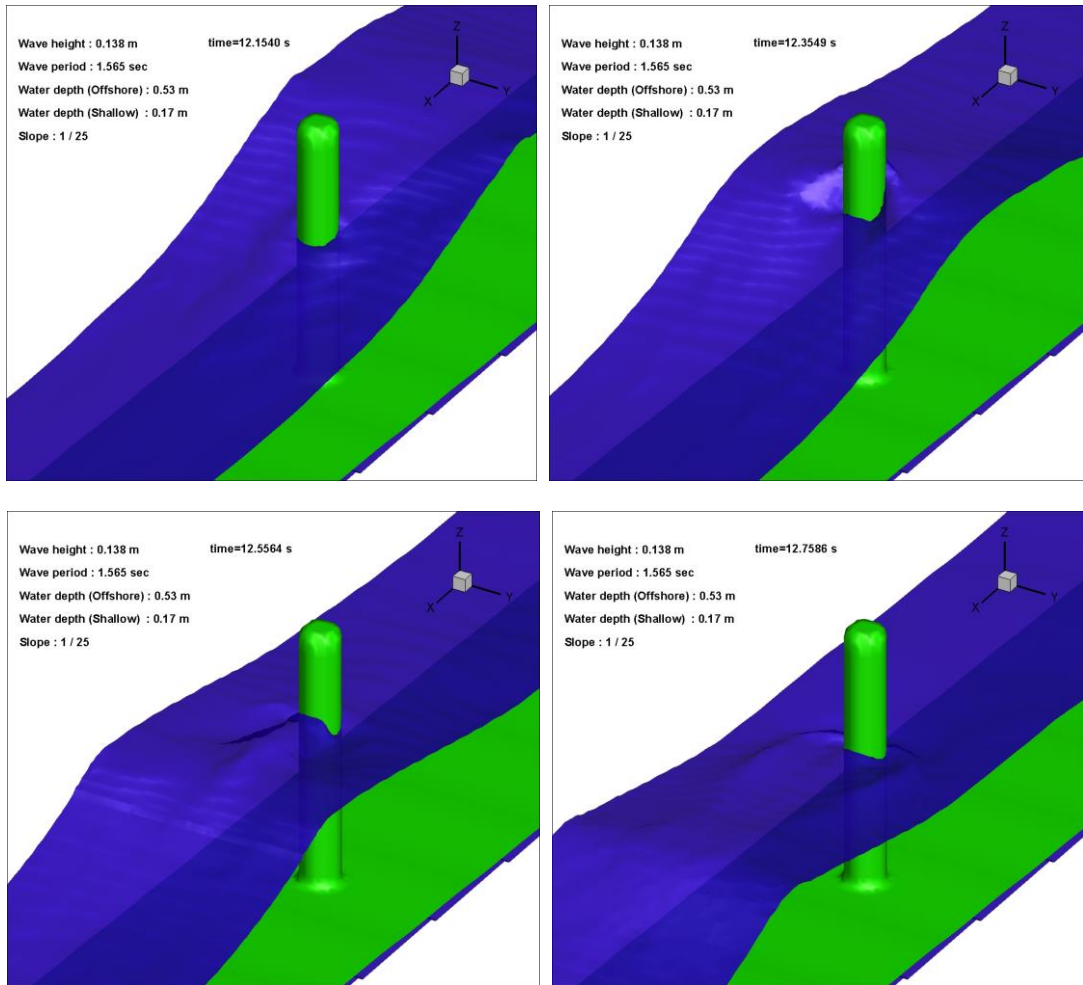


Fig. 8. Snapshots of the spatiotemporal variations for the instantaneous water levels (time =12.15 s, 12.35 s, 12.55 s, and 12.75 s).

The measured inline wave forces and the inline wave forces calculated by the Navier-Stokes solver are compared in Fig. 7. The ordinate in the figure is the inline wave force normalized by $\rho g H_i D^2$. The black lines represent the results calculated by the Navier-Stokes solver and the red open circles indicate the data measured by DHI. The computed inline wave forces were obtained by integrating the fluid pressure over the wetted surface of the cylindrical pile. The comparison reveals that the time variations for the computed inline wave forces are quite similar to the time variations for the measured inline wave forces, although there is a discrepancy at the troughs of the wave forces.

The discrepancy is explained as follows. First,

there was a discrepancy in how the total wave forces on the cylindrical pile were measured for experiments compared with the numerical analysis. In the experiments, the wave forces were measured by using a 3D forces gauge, which is located underneath the cylindrical pile; however, in the numerical analysis, the wave forces were obtained by integrating the pressure distribution over the wetted surface of the pile. Such a discrepancy would have had a slight effect on estimating the respective (measured and calculated) total wave forces. Second, this difference arose in terms of how the shape of the cylindrical pile was depicted in the wave tanks. The cylindrical pile that was used in the experiments was a true circle, but the cylindrical pile that was employed in the computational domain

was a polygon that was split in an arbitrary manner. Although the new application was based on the cut-cell method in order to correctly approximate the structure in the computational domain, the slight difference between experimental and numerical analyses would yield the slightly underestimated wave forces around the trough in the numerical simulation. The discrepancy could be improved by using finer grids, but this would lead to a long simulation. Finally, the computed dynamic pressures in the vicinity of still water levels (SWLs) would be slightly under-predicted compared with the measured results. However, comparisons between computed and measured pressures were not made in the present paper because the dynamic pressures near the SWLs were not measured in the experiments previously undertaken by DHI. Therefore, additional investigations are required to examine this. Despite these discrepancies, the overall results show a reasonable agreement with the experimental data, as shown in Fig. 7.

Fig. 8 shows snapshots of the spatiotemporal variations for instantaneous water levels (time =12.15 s, 12.35 s, 12.55 s, and 12.75 s), where the cylindrical pile and the sloping bottom are embodied by the new application. The nonlinear wave-structure interaction occurring in the vicinity of the cylindrical pile is simulated relatively well by the numerical model.

4. Conclusions

A 3D numerical model was proposed in the present study in order to estimate the free-surface elevation, water particle velocities, and nonlinear wave forces acting on a cylindrical pile installed on a sloping bottom. In addition to the 3D numerical model, the new application, which is based on the cut-cell method, has been used to easily install complicated obstacles in the computational domain. By comparing our experimental data with that obtained by DHI, the major conclusions can be summarized as follows:

- 1) The numerical model performed very well for estimating the free-surface elevation and water particle velocities (in the x-, y-, and z-directions) in the vicinity of the cylindrical pile on a sloping bottom, even for relatively steep wave conditions.
- 2) The computed inline wave forces agree reasonably well with the measured results, although the inline forces around the troughs are somewhat under-predicted compared with the measured values. It would be necessary to further investigate this discrepancy by using the pressure and velocity fields that are measured in the vicinity of the SWLs.
- 3) The applicability of the new application based on the cut-cell method is ideal. The nonlinear interaction between waves and structures is simulated relatively well in the vicinity of a cylindrical pile.
- 4) The proposed 3D numerical model is a useful tool that can predict the nonlinear wave forces on off-shore wind turbine foundations without the use of an empirical formula (i.e., Morison equation) or additional wave analysis models.

Acknowledgements

This research was supported by a grant (“stipendiat-TN-2008”) from the Research Council of Norway and two research projects “Development of Floating Wave Energy Converter activated by Pendulum” of Korea Institute of Ocean Science & Technology (KIOST) and “Development of OWC Wave Energy Utilization System” granted by the Ministry of Land, Transport and Maritime Affairs (MTLM). The physical model test data were provided by DHI.

References

- [1] Allied Engineering, *User's Manual for Advanced Parallel AMG Version 1.3*, Tokyo, (2011).
- [2] Amsden A.A, Harlow F.H, *A simplified MAC technique for incompressible fluid flow calculation*, Journal of Computational Physics, 6 (1970) 322-325.
- [3] API RP 2A-WSD, *Recommended Practice for Planning, Designing and Constructing Fixed Offshore Platforms – Working Stress Design*, Sections 1 & 2, American Petroleum Institute, Washington, USA, (2000).
- [4] Brorsen M, Larsen J., *Source generation of nonlinear gravity waves with the boundary integral equation method*, Coastal Engineering 11 (1987) 93-113.
- [5] CERC, *Shore Protection Manual*, Coastal Engineering Research Center, Corps of Engineers, U.S. Army, (1984).
- [6] Chen X, Li Y, Teng B., *Numerical and simplified methods for the calculation of the total horizontal wave force on a perforated caisson with a top cover*, Coastal Engineering 54 (2007) 67-75.

- [7] Choi S.J, Gudmestad O.T, *The effect of breaking wave induced currents on an offshore wind turbine foundation*. Fluid Structure Interaction VI:119-131, (2011).
- [8] Chun I.S, Shim J.S, Choi S.J., *Investigation on the design wave forces of ear-do ocean research station II: Fluid force in the breaking wave field*, Journal of the Korean Society of Coastal and Ocean Engineers, (2000) 168-180.
- [9] DnV-RP-C205, *Recommended Practice, Environmental Conditions and Environmental Loads*, 44, 52-53, DET NORSKE VERITAS, Oslo, Norway (2007).
- [10] Hinatsu M., *Numerical simulation of unsteady viscous nonlinear waves using moving grid systems fitted on a free surface*, J. Kansai Soc. Naval Archit., 217 (1992) 1-11.
- [11] Hirt C.W., Nichols B.D., *Volume of fluid method for the dynamics of free boundaries*, Journal of Computational Physics, 39(1) (1981) 201-225.
- [12] Hirt C.W, Sicilian J.M., *A porosity technique for the definition of obstacles in rectangular cell meshes*, Proceedings of the 4th International conference on Numerical Ship Hydrodynamics, Washington D.C., 1-10 (1985).
- [13] Hsu T.J., Sakakiyama T, Liu P.L-F., *A numerical model for wave motions and turbulence flows in front of a composite breakwater*. Coastal Engineering 46 (2002) 25-50.
- [14] ISO 19902, *Petroleum and natural gas industries – Fixed steel offshore structures*, CEM, Brussels, Belgium (2007).
- [15] Kawasaki K, Iwata K., *Numerical analysis of wave breaking due to submerged breakwater in three-dimensional wave fields*, Proceedings of the Conference of the American Society of Civil Engineers, Copenhagen, Denmark, 853-866, (1998).
- [16] Lee K.H., Mizutani N., *A numerical wave tank using direct-forcing immersed boundary method and its application to wave force on a horizontal cylinder*. Coastal Engineering Journal 51 (2009) 27-48.
- [17] Lee K.H., Park J.H., Baek D.J., Cho S., Kim D.S., *Discussion on optimal shape for wave power converter using oscillating water column*, Journal of the Korean Society of Coastal and Ocean Engineers 23(5) (2011) 345-357.
- [18] Roy D.J., Ghosh S., *Wave force on vertical submerged circular thin plat in shallow water*, Ocean Engineering 33 (2006) 1935-1953.
- [19] Smagorinsky J., *General circulation experiments with the primitive equation*. Monthly Weather Review 91(3) (1963) 99-164.
- [20] Walkden M.J., Wood D.J., Bruce T., Peregrine D.H., *Impulsive seaward loads induced by wave overtopping on caisson breakwaters*, Coastal Engineering 42 (2001) 257-276.